Yin, A.J.W. et al.: The neural vulnerabilities in reward processing in Gambling Disorder

https://doi.org/10.1556/2006.2025.00049

Supplementary Materials

METHODS

Experimental setup and MRI acquisition

Functional and structural brain images were acquired using a 3.0T Siemens MAGNETOM Prisma MRI scanner with a 32-channel phased-array head coil at the Center for Cognitive and Brain Sciences, University of Macau. The stimuli were projected through a rear-facing mirror mounted on top of the head coil from an LCD monitor (Inroom Viewing Device, NordicNeuroLab As) positioned 60 cm behind the scanner bore. To minimize head motion during the scanning, foam paddings were used to expand and fill gaps between the head and MRI coil. The stimuli were programmed to await a trigger signal ("s") using E-Prime 2.0 software. The trigger signal was sent from SyncBox (NordicNeuroLab AS) synchronously with the start of each functional scan. Participants' response was recorded by an MR-compatible response grip.

The fMRI experiment consisted of 4 functional task scans and 1 T1-weighted structural scan. The T1-weighted structural scan was assigned after the second functional scan. The functional task scans were acquired using the single-shot echo planar imaging (EPI) sequence. The imaging parameters were specified: 37 slices in interleaved ascending order, posterior-to-anterior (P-A) phase-encoding direction, TR = 2000 ms, TE = 30 ms, flip angle (FA) = 76°, field of view

(FOV) = 192 mm × 192 mm, matrix size = 64 × 64, voxel size = 3×3×3 mm; slices = 37, bandwidth = 2442 Hz/Px. Each functional task run contained 285 image volumes, with an effective scan time of 9.5 minutes. High-resolution T1-weighted anatomical structural images were obtained using the Magnetization-Prepared Rapid Gradient-Echo (MPRAGE) sequence, with the same center of slice group and orientation as the functional images. The imaging parameters were specified: FOV = 256 mm × 256 mm, acquisition matrix = 256 × 256, bandwidth = 200 Hz/Px, scan time = 540s, slice thickness = 1 mm.

fMRI behavioral data analysis

The fMRI behavioral data analysis involved examining reaction times and the frequency for each type of decision-making event (RD, SD, ND) as well as the corresponding reward events (RDwin, RDloss, SDloss, NDdouble, and NDwin). These variables were extracted and subjected to statistical analysis. The frequency of each event type was presented as a percentage (%), while response times were presented as mean ± standard deviation (SD). Comparative analyses were conducted using Pearson's chi-squared test ($\chi 2$) for categorical data. For continuous data, the Student's t-test was used for comparing two groups, and analysis of variance (ANOVA) was applied for comparing more than two groups.

fMRI data preprocessing

The quality of all imaging data was evaluated using visual inspection, customized versions of TSDiffAna (http://sourceforge.net/projects/spmtools/), and ArtRepair software (http://cibsr.stanford.edu/tools/human-brain-project/artrepair-software.html). The fMRI data

preprocessing and analyses were performed using (Statistical Parametric Mapping v12, SPM12; Wellcome Department of Cognitive Neurology, London, UK; https://www.fil.ion.ucl.ac.uk/spm/software/spm12/). The data preprocessing involved the following steps: (1) The first three images were removed to ensure the steady state of the blood-oxygen-level-dependent (BOLD) signal. (2) Slice-time correction was applied to synchronize the data on each slice to the same point in time. (3) The first image in the third scan was specified as a reference for realigning the timeseries of images acquired from the same subject, to obtain the highest probability of closely resembling the T1 image. The least squares approach was applied. The subject with head movement greater than half of voxel size (1.5 mm) was excluded from the subsequent statistical analysis. (4) The realigned functional images were coregistered to the T1 structural image using a rigid-body transformation. The three translations and three rotations parameters (rigid body) spatial transformations were evaluated as the inspection of head motion. (5) Then the images were spatially normalized into the Montreal Neurological Institute (MNI, Montreal, Canada) space and spatially smoothed with an 8-mm FWHM isotropic Gaussian kernel.

General linear model (GLM) analysis

For each subject, the effect of conditions on the BOLD signal was analyzed using the GLM model on a voxel-by-voxel basis. The Canonical Hemodynamic Response Function (HRF) was used to characterize the event-related responses, and six rigid-body transformation parameters were assigned as the regressors in the GLM model. For the decision-making process, 3 linear contrasts were created: SD, RD, ND. For the reward process, five linear contrasts were created: RDwin, RDloss, SDloss, NDdouble, NDwin. The GLM analysis yields partial *t*-statistic values

for each event type and contrast. Family-wise error (FWE) correction was applied for multiple comparisons at the cluster level, with the statistical threshold set at $p < 0.05$.

In the group-level statistical analysis, to assess the effect of diagnosis on the BOLD signal of the decision-making process, a two-way repeated-measures analysis of covariance (ANCOVA) with the between-subjects factors of diagnosis (GD vs. HC) and within-subject factors of decision (SD vs. RD vs. ND), with the education years and risk attitude scores (DOSPERT) as the covariates was conducted. To assess the effect of diagnosis on the BOLD signal of the reward process, a two-way repeated-measures ANCOVA specified the design metrics with the between-subjects factors of diagnosis (GD vs. HC) and within-subject factors of reward (RDwin vs. RDloss vs. SDloss vs. NDdouble vs. NDwin), with the education years and risk attitude scores (DOSPERT) as the covariates was conducted. Multiple comparison corrections were performed with a FWE rate of 0.05. Then Bonferroni post hoc test was applied, with significance set at $p < 0.05$.

Statistical maps illustration

For enhanced anatomical precision, the statistical maps were rendered onto the cortical surface using the Analysis of Functional Neuroimages/AFNI Surface Mapper (AFNI/SUMA) programs (National Institute of Mental Health, Bethesda, Maryland, United States: http://afni.nimh.nih.gov/afni), employing the MNI152 template.

Functional regions of interest (ROIs) extraction and post-hoc analysis

For further analysis, the ROIs were identified based on the significant functional activations triggered by the events. The definition of cluster ROIs was guided by several references, including the Human Capital Planning (HCP) Template (Yeh, 2022), Automated Anatomical Atlas (AAL) template (Rolls, Huang, Lin, Feng, & Joliot, 2020; Tzourio-Mazoyer et al., 2002), CsurfMaps (Sereno, Sood, & Huang, 2022), and previous literature (Fliessbach et al., 2007; Reuter et al., 2005). Activation clusters were selected in SPM based on statistical peak values and thresholds. ROIs were isolated as distinct regions by gradually increasing the statistical threshold if the clusters extended across the areas defined in templates; the cluster size and corresponding statistical thresholds are detailed in Table S2. Masks for each ROI were generated using the MarsBar tool for SPM (http://marsbar.sourceforge.net/). The beta weights from the GLM analysis for each condition were extracted, followed by a Bonferroni post-hoc test with a significance level of $p < 0.05$. The HRF timeseries were extracted from each event-onset, extending up to 20 seconds (10 TRs). The amplitude of BOLD signal changes was calculated and averaged across the group samples.

Within-subject multivoxel pattern analyses (MVPA)

In addition to analyzing the univariate BOLD changes at the single voxel level, we examined distributed activity patterns across the ROIs. MVPA was employed to decode the neural representation patterns related to decision-making and reward processing in both the GD and HC groups. Preprocessing included slice timing correction on the raw functional data. For each subject, single-trial estimates of the hemodynamic response function (HRF) and six rigid-body transformation regressors were included as nuisance regressors to obtain voxel-wise beta weight values. Then, GLM analyses were conducted separately to model decision and reward

conditions. The single-trial beta weights in ROIs were extracted and normalized using Z-transform for the subsequent ROI analysis.

MVPA was performed using The Decoding Toolbox (TDT) (Hebart, Görgen, & Haynes, 2014). Decoding was performed within spheres with a radius of 3 voxels, using the ROI mask generated in the previous step. The single-trials beta weights labeled with RDwin and RDloss were submitted to trained using a one-vs.-one multiclass support vector machine (SVM) (Cortes & Vapnik, 1995) classification approach . The leave-one-run-out cross-validation was performed and the training sets and testing sets ratio is around 3:1 due to random selection. For each participant, the confusion matrix, comparing the frequency of predicted labels with true labels for each participant, was created. For the group-level analysis, one-sample *t*-test was used to compare the accuracy of conditions against chance, and two-sample *t*-tests were employed to investigate whether different neural representations could classify GD and HC under the same conditions. We computed 95% confidence intervals (95% CI) for each comparison. Effect sizes for the *t*-tests were calculated using Cohen's d at the 95% confidence level.

The dynamic timeseries classification

The percentage changes in the BOLD signals for each trial from the time of reward onset to 10 TRs thereafter were extracted using Marsbar (version 0.45) (Brett, Anton, Valabregue, & Poline, 2002). Subsequently, the MVPA-Light package (Treder, 2020) was utilized to decode the BOLD signal percentage changes around the diagnosis (GD vs. HC) at a between-subjects level for each condition (**Figure S4**). The BOLD values of RDwin, labeled as GD or HC at the same point from the stimulus onset (e.g., all BOLD values at the 1st TR of the RDwin-reward onset in both GD and HC groups), were extracted and submitted into SVM classifiers. A five-fold cross-

validation scheme (with a training-to-testing set ratio of 4:1), repeated five times, was employed. The same procedure was then applied to the BOLD values at each time point for both RDwin and RDloss conditions. The classification performances were represented by the area under the curve (AUC) values. The performance test for binary classification across time was conducted using nonparametric Wilcoxon tests at each time point. The null AUC value was set at a chance level of 0.5, with the reference distribution computed from 1,000 random draws. The significance threshold was set at $p < 0.05$.

RESULTS

The demographic and clinical characteristics of participants

The demographic and clinical characteristics of GD and HC are presented in **Table S1**. There was no significant difference in the demographic characteristics of age (t = 0.807, $p = 0.421$), sex distribution ($\chi2 = 0.442$, $p = 0.506$) or BMI (t = 0.964, $p = 0.337$). However, they differed in terms of education years (t = 2.907, $p = 0.004$) and thus it was included as a covariate in subsequent analyses. There were no significant discrepancies in the clinical characteristics, including age of first gambling experience (t = 0.238, $p = 0.812$), duration of gambling experience (t = 0.093, $p = 0.925$), HAM-A score (t = 0.602, $p = 0.548$), HAM-D scores (t = 0.894, $p = 0.373$), and total score of DOSPERT (t = 0.852, $p = 0.396$). Notably, significant deviations were observed in the GD-YBOCS scores (t = 5.361, $p = 7.708E-07$) indicating differing severity levels of additional gambling between the GD and HC groups.

Behavioral performance characteristics in the task

The fMRI behavioral data analysis encompassed response times (RT) and frequencies for each type of decision-making (RD, SD, ND). A similar behavioral pattern in RTs and frequencies was observed in both GD and HC groups. Increased tendencies in RTs were observed from ND to RD to SD in both the GD and HC groups. However, only the difference in the comparison of ND and RD in the HC group survived the Bonferroni correction ($t = 3.54$, $p = 0.01$, Bonferroni corrected), as shown in **Figure S1A, Table S2.** Additionally, a decrease in frequency was observed from RD to SD in both HC and GD groups, as shown in **Figure S1B, Table S2.** Significant differences were found in the comparison of RD and SD in the HC group ($t = 3.67$, $p = 6.87E-03$, Bonferroni corrected). However, no differences were observed in the comparisons of frequency among reward types (all $p > 0.05$) (**Figure S1C, Table S2**).

The neural activation pattern for decision-making and reward of task

To investigate the specific neural representations in GD for the decision and reward processes, two independent GLM analyses were conducted within the GD and HC groups. Each analysis was separately time-locked to the onset of the decision stage and reward stage. Subsequently, a repeated measures ANCOVA was applied in the group analysis, with education years and risk attitude scores (DOSPERT) as covariates.

First, the main effect of the decision and reward processing on the BOLD signal was examined. A significant decision main effect was observed in the left anterior part of the insula (aInsula) ($F = 17.57$, $p = 1.70E-03$, FWE corrected), right aInsula ($F = 16.21$, $p = 4.92E-03$, FWE corrected), and dorsal medial part of the dorsolateral prefrontal cortex (dmPFC) ($F = 15.76$, $p = 6.98E-03$, FWE corrected). To further identify the sources of these significant

differences, the Bonferroni post-hoc test was applied. In the decision process, the most significant differences were observed in the RD condition compared to the ND condition in the ROIs of the left and right aInsula, as well as the right dmPFC, both in the GD group and the HC group ($p < 0.01$, Bonferroni corrected) (refer to **Table S2** for detailed coordinate locations and statistical results, and **Figure S1**, **Figure S2A** for illustrations). However, no significant difference was observed in the main effect of diagnosis on decision processing and the Diagnosis × Decision interaction ($p > 0.05$).

A significant main effect of reward processing was detected in several brain regions after FWE correction with a threshold of 0.05, including the bilateral aInsula, a cluster containing the right inferior frontal gyrus and middle frontal gyrus (IFG/MFG), a cluster containing the dorsal medial part of the dorsolateral prefrontal cortex and bilateral dorsal part of the anterior cingulate cortex (dmPFC/dACC), the right superior frontal gyrus (SFG), the bilateral ventral striatum (VS), the right anterior part of the posterior cingulate cortex (aPCC), the right temporoparietal junction (TPJ), and the right dorsolateral prefrontal cortex (dlPFC). The main effect of the reward processing on the BOLD signal activation is illustrated in **Figure S1 B,** and the coordinates of peak voxel and statistic values are listed in **Table S2.** In the post-hoc analysis, the overall activation pattern exhibited a gradient of increased signal effect in the RDwin and RDloss conditions compared to the other three conditions (SDloss, NDdouble, and NDwin), in both the GD and HC groups (as shown in **Figure S2 B**).

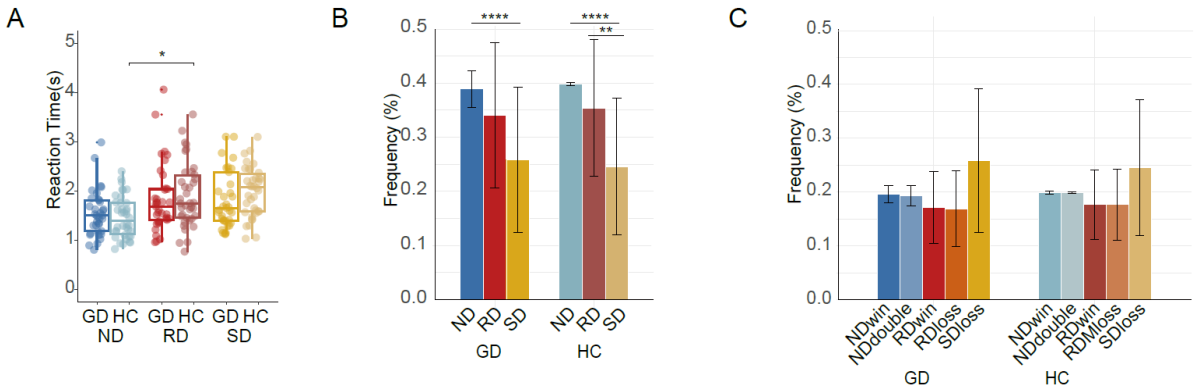

Figure S1. Behavioral performance in the task

*(A) The comparison examines differences in response times for each type of decision (RD, SD, ND). The displays the median with the interquartile range (25% to 75%) represented by the boxes, while the whiskers extend to the minimum and maximum data points, excluding extreme values. Outlier points, plotted individually, indicate extreme data. Significantly increased reaction time was shown in the comparison of ND to RD in the HC group after (t = 3.54, p = 0.01, Bonferroni corrected). (B) The comparison investigates differences in frequency for each type of decision (RD, SD, ND). Histograms and error bars show the mean and standard deviation of percentages (%) in each response type. A significant decrease in frequency (%) was observed in the comparison of ND to SD in both the HC and GD groups (t = 3.54, p = 0.01, Bonferroni corrected), as well as in the comparison of RD to SD in the GD group (t = 7.33, p = 1.82E-07, Bonferroni corrected). (C) The comparison explores differences in frequency for each type of reward (RDwin, RDloss, SDloss, NDdouble, and NDwin). Mean ± SD percentages are shown for each response type (all P > 0.05). Significance levels are denoted as follows: *p < 0.05, **p < 0.01, ***p < 0.001, ****p < 0.0001, with all p-values in the figure subjected to multiple corrections. GD, gambling disorder; HC, healthy controls.*

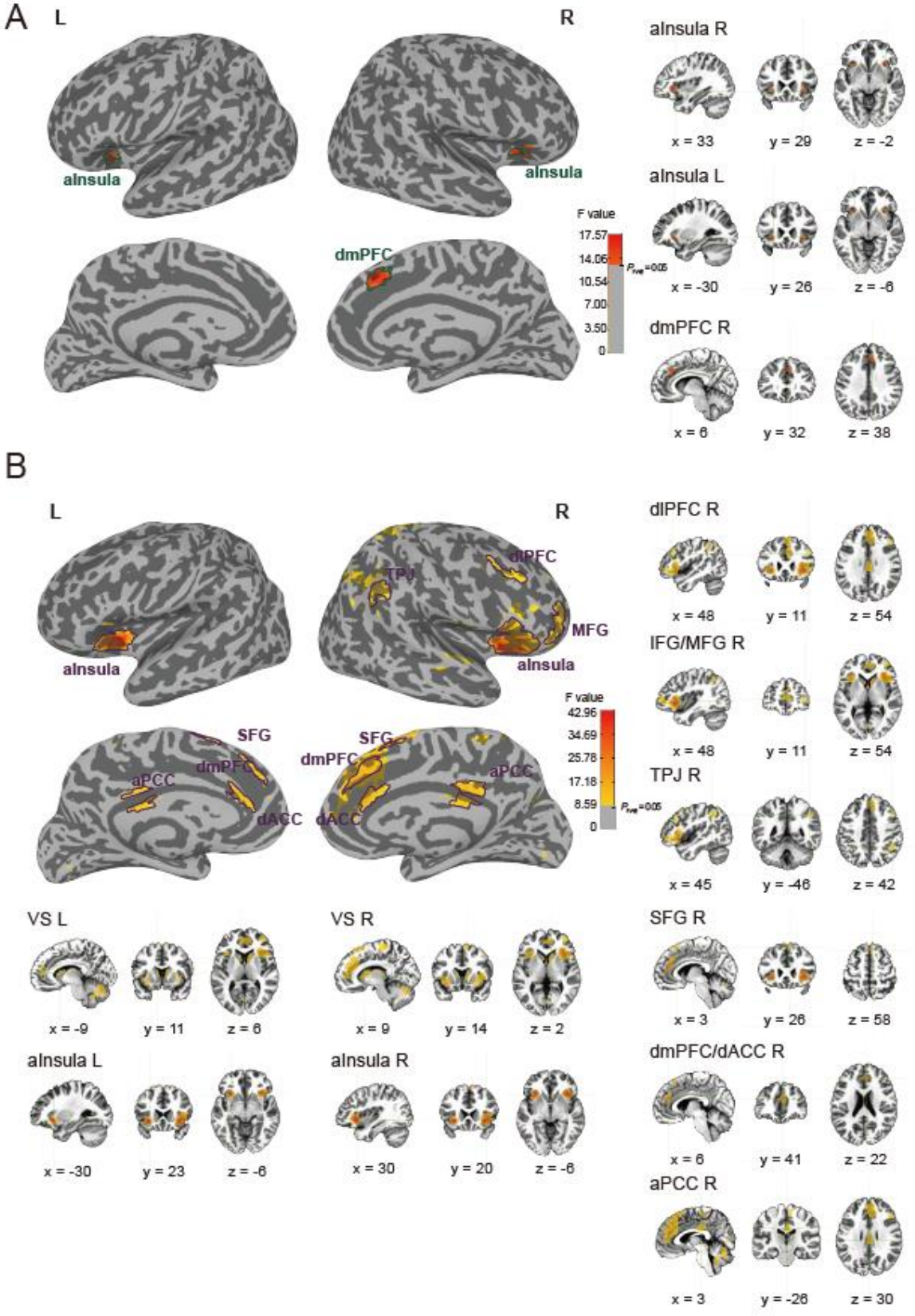
A
L
R
aInsula
aInsula
dmPFC
F value
17.57
14.06
10.54
7.00
3.50
0
aInsula R
x = 33
y = 29
z = -2
aInsula L
x = -30
y = 26
z = -6
dmPFC R
x = 6
y = 32
z = 38
B
L
R
aInsula
TPJ
dlPFC
MFG
aInsula
SFG
dmPFC
aPCC
dACC
SFG
dmPFC
aPCC
dACC
F value
42.96
34.69
25.78
17.18
8.59
0
dlPFC R
x = 48
y = 11
z = 54
lFG/MFG R
x = 48
y = 11
z = 54
TPJ R
x = 45
y = -46
z = 42
VS L
x = -9
y = 11
z = 6
VS R
x = 9
y = 14
z = 2
SFG R
x = 3
y = 26
z = 58
aInsula L
x = -30
y = 23
z = -6
aInsula R
x = 30
y = 20
z = -6
dmPFC/dACC R
x = 6
y = 41
z = 22
aPCC R
x = 3
y = -26
z = 30

Figure S2. The neural activation pattern for the main effect of decision and reward

The activation cluster for the main effect of the decision in the surface localization is shown in (A), and the peak values in voxel-based coordination are depicted in (B). The main activated clusters for the main effect of reward in the surface localization are shown in (C), and the peak values in voxel-based coordination in (D). All comparisons were FWE corrected with the threshold of $p < 0.05$.

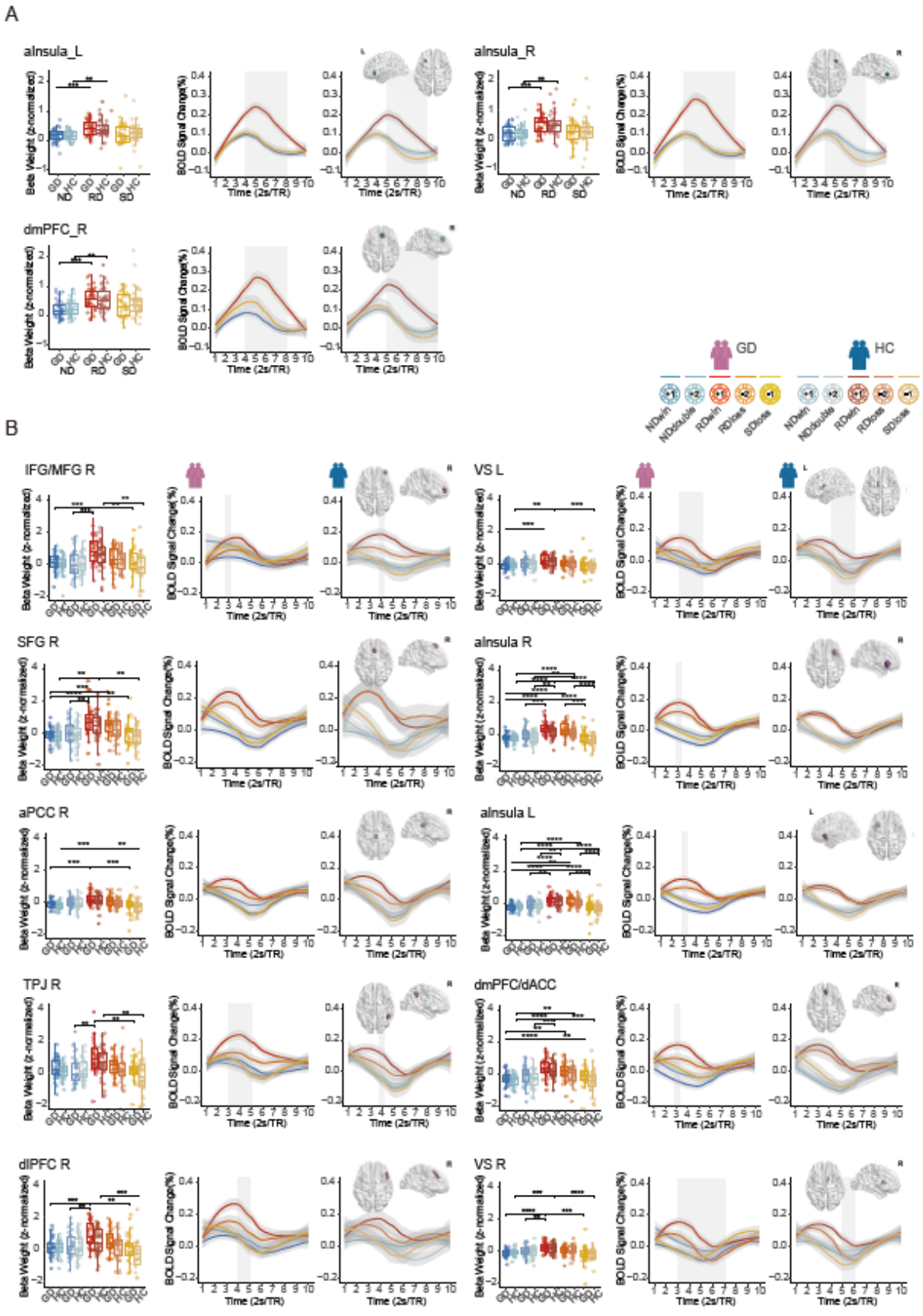
A
aInsula_L
aInsula_R
dmPFC_R
GD
HC
NDwin
NDdouble
RDwin
RDloss
SDloss
B
IFG/MFG R
VS L
SFG R
aInsula R
aPCC R
aInsula L
TPJ R
dmPFC/dACC
dlPFC R
VS R
Beta Weight (z-normalized)
BOLD Signal Change(%)
Time (2s/TR)

Figure S3. The post-hoc analysis and the timeseries for the activation regions in the main effect of reward

(A) The post-hoc analysis and timeseries for the activation regions in the main effect of decision. (B) The post-hoc analysis and timeseries for the activation regions in the main effect of reward. The boxplot represents the median and the interquartile range of the beta weights for each condition in the GLM analysis, and the scatters represent the beta weights for individuals. The groups are illustrated with different color labels, as shown in the top-right of plot (B). All comparisons were corrected by the Bonferroni correction. The gray background indicates a significant difference in the timeseries at the corresponding time points between the RDloss and RDwin conditions, $p < 0.05$.

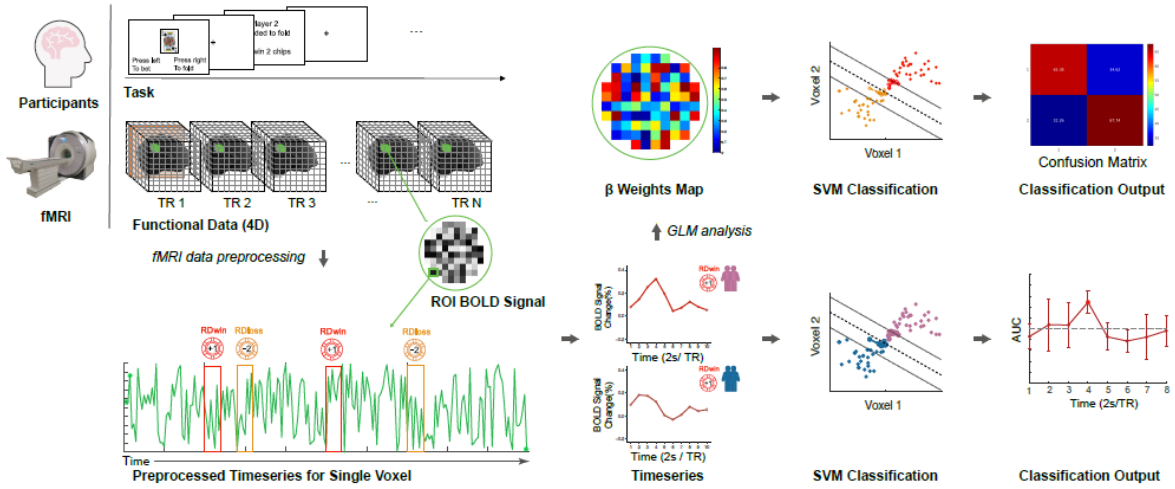

Figure S4 The scheme of the classification analysis.

The task-related fMRI data were obtained, and single-trial timeseries for ROIs were extracted, as illustrated in the left part of the figure. For the within-subject multivoxel pattern analyses (shown in the upper-right part of the figure), beta weight coefficients derived from the GLM analysis were utilized for classification. A one-vs-one multiclass SVM classifier was applied, producing confusion matrices for RDloss and RDwin conditions for each subject. These matrices were subsequently used in the group-level analysis. For the dynamic time-series classification (shown in the lower-right part of the figure), the timeseries of RDloss (or RDwin) conditions, labeled as GD or HC at the same time point from the stimulus onset, were extracted and submitted into SVM classifiers. AUC values were calculated for each time point. Abbreviation: fMRI, Functional magnetic resonance imaging; ROI, Region of interest; SVM, support vector machine; TR: Repetition Time.

Table S1 The demographic and clinical characteristics in GD and HC groups

Variables	N	GD	HC	Statistical tests	*p*
Age (Years, Mean ± SD)	50/53	36.18±11.69	34.32±11.67	t = 0.807	0.421
Sex (NO. Male/Female)	50/53	43/7	43/10	$\chi 2$= 0.442	0.506
BMI (Weight(kg)/High(cm)2, Mean ± SD)	50/53	23.92±3.60	23.24±3.55	t = 0.964	0.337
Education (Years, Mean ± SD)	50/53	11.68±2.96	13.42±3.09	t = 2.907	0.004
Age of first gambling experience (Years, Mean ± SD)	50/29	23.24±8.12	23.72±9.65	t = 0.238	0.812
Duration of gambling experience (Years, Mean ± SD)	50/29	13.58±10.37	13.34±11.40	t = 0.093	0.925
Age onset for pathological gambling (Years, Mean ± SD)	46/ -	25.71±8.91	-	-	-
Duration for pathological gambling (Years, Mean ± SD)	46/ -	10.83±10.48	-	-	-
Duration of abstinence from gambling (Months, Mean ± SD)	7/ -	6.85±4.25	-	-	-
Frequence (Times per week in lasted one year, Mean ± SD)	49/30	3.30±3.87	1.83±2.03	t = 1.922	0.058
Maximum Amount for betting (MOP, Mean ± SD)	48/30	33504±14642	14185±45511	t = 1.196	0.235
Monthly spending in gambling (MOP, Mean ± SD)	28/10	13714±18628	6300±11937	t = 1.169	0.25
DSM-5 criteria (Mean ± SD)	48/24	5.62±2.19	1.70±1.42	t = 7.915	2.61E-11
PG-YBOCS (Mean ± SD)	45/23	24.93±7.05	15.73±5.47	t = 5.461	7.71E-07
HAM-A (Mean ± SD)	45/41	4.8±6.01	4.02±5.90	t = 0.602	0.548
HAM-D (Mean ± SD)	45/41	4.33±5.68	3.26±5.31	t = 0.894	0.373
IQ (Mean ± SD)	46/43	21.80±12.42	24.83±10.01	t = 1.26	0.210
DOSPERT (Mean ± SD)					
Total scores	48/48	101.83±25.52	97.14±28.28	t = 0.852	0.396
Ethical subscore	48/48	17±7.01	12.72±5.29	t = 3.365	0.001
Financial subscore	48/48	24.29±7.96	21.27±8.56	t = 1.789	0.076
Health/Safety subscore	48/48	17.85±5.82	17.14±6.84	t = 0.546	0.586
Recreational subscore	48/48	16.77±8.11	21.41±9.99	t = 2.49	0.014
Social subscore	48/48	25.91±6.15	24.58±6.424	t = 1.038	0.301

Abbreviation: GD, Gambling disorder; HC, Healthy controls SD,Standard deviation; BMI,Body mass index; HAM-A, Hamilton Anxiety Rating Scale; HAM-D,Hamilton Depression Rating Scale; PG-YBOCS, Yale Brown Obsessive Compulsive Scale adapted for Pathological Gambling; DSM-5, The Diagnostic and Statistical Manual of Mental Disorders, Fifth Edition; IQ, Intelligence Quotient; DOSPERT, Domain-Specific Risk-Taking.

Table S2 Behavioral performance in GD and HC groups

Stages/Conditions	Comparations	RT					Frequency				
		GD (N=38)	HC (N=40)	t	*p*	*p#*	GD (N=37)	HC (N=40)	t	*p*	*p#*
Decision											
ND		1.680±0.997	1.467±0.417	1.20	0.236	1	0.398±0.003	0.389±0.034	1.60	0.117	1
RD		1.833±0.685	1.913±0.654	-0.52	0.603	1	0.353±0.126	0.340±0.133	0.44	0.665	1
SD		2.086±1.424	2.354±2.364	-0.60	0.553	1	0.245±0.126	0.258±0.133	-0.42	0.676	1
	GD ND vs. RD	/	/	-0.77	0.446	1	/	/	2.13	0.04	0.6
	GD ND vs. SD	/	/	-1.42	0.161	1	/	/	7.33	1.21E-08	1.82E-07
	GD RD vs. SD	/	/	-0.97	0.335	1	/	/	3.67	4.58E-04	6.87E-03
	HC ND vs. RD	/	/	-3.54	0.0008	1.13E-02	/	/	2.16	0.037	0.555
	HC ND vs. SD	/	/	-2.28	0.028	0.42	/	/	5.83	7.12E-07	1.07E-05
	HC RD vs. SD	/	/	-1.11	0.275	1	/	/	2.68	0.009	0.135
Reward											
NDdouble		/	/	/	/	/	0.198±0.002	0.195±0.015	1.11	0.273	1
NDwin		/	/	/	/	/	0.199±0.001	0.193±0.019	1.96	0.058	1
RDwin		/	/	/	/	/	0.176±0.065	0.169±0.070	0.49	0.628	1
RDloss		/	/	/	/	/	0.177±0.064	0.171±0.066	0.36	0.717	1
SDloss		/	/	/	/	/	0.245±0.126	0.258±0.133	-0.42	0.676	1
	GD NDdouble vs. RDwin	/	/	/	/	/	/	/	2.02	0.051	1
	GD NDdouble vs. RDloss	/	/	/	/	/	/	/	2.04	0.049	1
	GD RDwin vs. RDloss	/	/	/	/	/	/	/	-0.01	0.991	1
	GD NDwin vs. RDloss	/	/	/	/	/	/	/	2.12	0.041	1
	GD NDwin vs. RDwin	/	/	/	/	/	/	/	2.10	0.043	1
	GD NDwin vs. NDdouble	/	/	/	/	/	/	/	1.49	0.143	1
	HC NDwin vs. NDdouble	/	/	/	/	/	/	/	-0.57	0.569	1

HC NDwin vs. RDwin	/	/	/	/	/	/	/	2.05	0.046	1
HC NDwin vs. RDloss	/	/	/	/	/	/	/	1.96	0.057	1
HC NDdouble vs. RDwin	/	/	/	/	/	/	/	2.27	0.029	0.812
HC NDdouble vs. RDloss	/	/	/	/	/	/	/	2.19	0.034	0.952
HC RDwin vs. RDloss	/	/	/	/	/	/	/	-0.15	0.883	1

Abbreviation: GD, Gambling disorder; HC, Healthy controls; RT, reaction time; SD,Standard deviation; RD,risky decision; SD,safty decision; ND,non-decision; RDwin,risky decision win of $2; RDloss, risky decision loss of $2; SDloss, safty decision loss of $1; NDdouble, non-decision gain of $2, Ndwin, non-decision gain of $1.p#: corrected *p* value.

Table S3 the neural activation for the effects of the simplified poker game task

	R/L	Peak F value	*p* (FWEcorr)	*p* (uncorr)	x	y	z	k(E)
Decision phase GD(N=38) versus HC(N=40)								
Main effect of diagnosis								
No significant cluster								
Main effect of Decision (FWE *p* < 0.05)								
Insula	L	17.57	1.70E-03	8.23E-08	-30	26	-6	8
Insula	R	16.21	4.92E-03	2.69E-07	33	29	-2	20
dmPFC	R	15.76	6.98E-03	3.98E-07	6	32	38	23
Diagnosis × Decision interaction								
No significant cluster								
Reward phase GD (N=37) versus HC(N=40)								
Main effect of diagnosis (FWE *p* < 0.05)								
LIP (Cluster 1)	L	38.98	3.35E-05	1.31E-09	-39	-52	54	42
aInsula	R	30.52	1.21E-03	6.70E-08	42	20	-6	28
aPCC	L	29.91	1.57E-03	8.90E-08	-3	-4	38	8
SFG	L	24.80	1.38E-02	1.03E-06	-3	50	38	8
LIP (Cluster 2)	L	23.57	2.33E-02	1.86E-06	-21	-61	46	5
IFG	R	23.40	2.49E-02	2.02E-06	48	35	2	5
Main effect of Reward (FWE *p* < 0.05)								
Insula (combined a part of Operculum)	R	42.96	0.00	4.44E-16	36	20	-6	480
IFG/MFG	R	10.80	7.31E-04	3.07E-08	39	53	6	15
aInsula	L	41.06	0.00	4.44E-16	-30	23	-6	202
dmPFC/dACC	L/R	19.90	3.73E-10	1.09E-14	6	41	22	624
SFG	R	17.41	1.96E-08	5.60E-13	3	26	58	NA
VS	R	17.86	9.51E-09	2.72E-13	9	14	2	81
aPCC	R	13.89	3.77E-06	7.60E-11	3	-22	30	86
VS	L	11.34	3.15E-04	1.22E-08	-9	11	6	22
TPJ	R	9.62	4.43E-03	2.25E-07	45	-46	42	60
dlPFC	R	9.60	4.58E-03	2.33E-07	48	11	54	49
Diagnosis × Reward interaction								
No significant cluster								

Abbreviation: R, right; L, left; aInsula, anterior insula; VS,ventral striatum; vmPFC,ventromedial prefrontal cortex; aInsula,anterior insula; dlPFC, dorsolateral prefrontal cortex; dACC, dorsal part of anterior cingulate cortex; dmPFC, dorsal medial part of dorsolateral prefrontal cortex; LIP, lateral intraparietal sulcus; SFG, superior frontal gyrus, MFG, middle frontal gyrus; IFG, inferior frontal gyrus; aPCC, anterior cingulate cortex; dPCC, posterior cingulate cortex; TPJ, temporoparietal junction; FWE, Family-wise error

Table S4 the classification accuracies for the RDloss an Rdwin conditions

Conditions	ROIs	GD					HC					GD vs. HC			
		Accuracies (%)	t	*p*	Cohen's *d*	95% CI	Accuracies (%)	t	*p*	Cohen's *d*	95% CI	t	*p*	*pcorr*	95% CI
RDloss															
	aInsula R	58.09±16.35	2.53	1.82E-02	0.50	1.495, 14.70	51.50±16.91	0.61	0.607	0.09	7.405, 0.089	1.52	0.134	0.538	-2.10, 15.28
	IFG R	71.00±24.94	4.29	2.33E-04	0.84	10.93, 31.08	47.11±36.05	0.64	0.644	-0.08	9.697, -0.07	2.89	0.005	0.022	7.33, 40.45
	SFG L	63.79±27.46	2.56	1.69E-02	0.50	2.701, 24.88	43.63±38.21	0.34	0.338	-0.17	6.962, -0.16	2.28	0.027	0.106	2.43, 37.89
	aPCC	65.43±27.61	2.85	8.63E-03	0.56	4.281, 26.58	43.72±39.44	0.36	0.360	-0.16	7.486, -0.15	2.39	0.020	0.080	3.54, 39.87
RDwin															
	aInsula R	44.33±16.93	-1.71	1.00E-01	-0.33	-12.5, 1.171	55.34±16.43	0.07	0.067	0.33	11.07, 0.325	-2.54	0.014	0.055	-19.7, -2.33
	IFG R	30.55±29.17	-3.40	2.27E-03	-0.67	-31.2, -7.66	51.47±36.30	0.81	0.814	0.04	14.14, 0.040	-2.40	0.019	0.078	-38.3, -3.49
	SFG L	33.41±28.67	-2.95	6.82E-03	-0.58	-28.1, -5.00	53.13±38.65	0.64	0.639	0.08	16.62, 0.081	-2.18	0.033	0.133	-37.8, -1.62
	aPCC	29.11±24.84	-4.29	2.37E-04	-0.84	-30.9, -10.8	53.63±38.16	0.58	0.583	0.10	16.94, 0.095	-2.84	0.006	0.025	-41.7, -7.26

Abbreviation: GD, Gambling disorder; HC, Healthy controls; RDwin,risky decision win of $2; RDloss, risky decision loss of $2; ROIs, Regions of interest. 95%CI, 95% Confidence Interval.

Table S5 The dynamic classification accuracies for the GD and HC groups during reward of RD

ROIs	Conditions	Accuracies (%)	TRs							
			1	2	3	4	5	6	7	8
IFG										
	RDloss	Accuracies (%)	0.59±0.06	0.62±0.11	0.66±0.10	0.49±0.16	0.43±0.10	0.53±0.19	0.58±0.21	0.41±0.18
		p	0.145	0.091	0.027	0.556	0.75	0.342	0.194	0.811
	Rdwin	Accuracies (%)	0.42±0.11	0.53±0.24	0.53±0.20	0.75±0.11	0.42±0.12	0.38±0.10	0.42±0.20	0.48±0.13
		p	0.784	0.365	0.342	0.003	0.807	0.886	0.804	0.598
SFG										
	RDloss	Accuracies (%)	0.39±0.07	0.49±0.20	0.50±0.21	0.48±0.14	0.35±0.14	0.66±0.11	0.48±0.21	0.45±0.16
		p	0.806	0.511	0.493	0.544	0.888	0.096	0.547	0.652
	Rdwin	Accuracies (%)	0.43±0.26	0.29±0.17	0.43±0.26	0.43±0.23	0.65±0.18	0.39±0.24	0.40±0.21	0.60±0.16
		p	0.705	0.948	0.694	0.69	0.101	0.764	0.785	0.228
aInsula R										
	RDloss	Accuracies (%)	0.50±0.23	0.53±0.08	0.64±0.10	0.47±0.19	0.48±0.12	0.55±0.16	0.68±0.17	0.5±0.21
		p	0.457	0.361	0.07	0.563	0.521	0.285	0.039	0.518
	Rdwin	Accuracies (%)	0.26±0.08	0.43±0.20	0.46±0.11	0.48±0.09	0.35±0.08	0.49±0.11	0.39±0.18	0.41±0.14
		p	0.994	0.72	0.638	0.576	0.924	0.49	0.838	0.769
aPCC										
	RDloss	Accuracies (%)	0.35±0.20	0.60±0.22	0.73±0.17	0.58±0.25	0.56±0.21	0.49±0.15	0.51±0.09	0.42±0.08
		p	0.905	0.166	0.015	0.224	0.235	0.515	0.477	0.764
	Rdwin	Accuracies (%)	0.57±0.16	0.56±0.12	0.58±0.26	0.54±0.20	0.64±0.12	0.58±0.11	0.54±0.17	0.42±0.10
		p	0.217	0.278	0.215	0.335	0.1	0.206	0.336	0.762

Abbreviation: GD, Gambling disorder; HC, Healthy controls; TR, repetition time; RDwin,risky decision win of $2; RDloss, risky decision loss of $2; ROIs, Regions of interest; SFG, superior frontal gyrus; IFG, inferior frontal gyrus; aPCC, anterior cingulate cortex; FWE, Family-wise error.

References

Brett, M., Anton, J.-L., Valabregue, R., & Poline, J.-B. (2002). *Region of interest analysis using an SPM toolbox.* Paper presented at the 8th international conference on functional mapping of the human brain.

Cortes, C., & Vapnik, V. (1995). Support-vector networks. *Machine learning, 20*, 273-297.

Fliessbach, K., Weber, B., Trautner, P., Dohmen, T., Sunde, U., Elger, C. E., & Falk, A. (2007). Social comparison affects reward-related brain activity in the human ventral striatum. *Science, 318*(5854), 1305-1308. doi:10.1126/science.1145876

Hebart, M. N., Görgen, K., & Haynes, J. D. (2014). The Decoding Toolbox (TDT): a versatile software package for multivariate analyses of functional imaging data. *Front Neuroinform, 8*, 88. doi:10.3389/fninf.2014.00088

Reuter, J., Raedler, T., Rose, M., Hand, I., Gläscher, J., & Büchel, C. (2005). Pathological gambling is linked to reduced activation of the mesolimbic reward system. *Nature Neuroscience, 8*(2), 147-148. doi:10.1038/nn1378

Rolls, E. T., Huang, C. C., Lin, C. P., Feng, J., & Joliot, M. (2020). Automated anatomical labelling atlas 3. *Neuroimage, 206*, 116189. doi:10.1016/j.neuroimage.2019.116189

Sereno, M. I., Sood, M. R., & Huang, R. S. (2022). Topological Maps and Brain Computations From Low to High. *Front Syst Neurosci, 16*, 787737. doi:10.3389/fnsys.2022.787737

Treder, M. S. (2020). MVPA-Light: A Classification and Regression Toolbox for Multi-Dimensional Data. *Front Neurosci, 14*, 289. doi:10.3389/fnins.2020.00289

Tzourio-Mazoyer, N., Landeau, B., Papathanassiou, D., Crivello, F., Etard, O., Delcroix, N., . . . Joliot, M. (2002). Automated anatomical labeling of activations in SPM using a

macroscopic anatomical parcellation of the MNI MRI single-subject brain. *Neuroimage, 15*(1), 273-289. doi:10.1006/nimg.2001.0978

Yeh, F. C. (2022). Population-based tract-to-region connectome of the human brain and its hierarchical topology. *Nat Commun, 13*(1), 4933. doi:10.1038/s41467-022-32595-4